ФИЗИКА ЭЛЕМЕНТАРНЫХ ЧАСТИЦ И АТОМНОГО ЯДРА
2004. Т. 35. ВЫП. 5

УДК 539.12

MEASUREMENTS IN CONDITIONS OF A VERY HIGH MULTIPLICITY

*O. L. Kodolova**

Moscow State University, Nuclear Physics Institute, Moscow
CERN, Geneva, Switzerland

*E-mail: Olga.Kodolova@cern.ch

ФИЗИКА ЭЛЕМЕНТАРНЫХ ЧАСТИЦ И АТОМНОГО ЯДРА
2004. Т. 35. ВЫП. 5

УДК 539.12

MEASUREMENTS IN CONDITIONS OF A VERY HIGH MULTIPLICITY

O. L. Kodolova[*]

Moscow State University, Nuclear Physics Institute, Moscow
CERN, Geneva, Switzerland

The Large Hadronic Collider will provide 14 TeV proton–proton beams and nucleus–nucleus collisions with the energy of 5.5–7 TeV/nucleon. High multiplicity events and high luminosity will force one to work in the condition of the strongly occupied tracker and calorimeter detectors. The development of methods of jet finding and jet energy correction which are tolerant to the occupancy and nonlinearity of calorimeter response is extremely important. Jet reconstruction and correction in CMS detector in pp and heavy ion events are considered. The main attention is payed to the new perspective method to correct jet energy using combined information from calorimeters and tracker detectors and to the background subtraction algorithm. A set of measurements that can be carried out in the case of heavy ion collisions, such as jet quenching and quarkonia suppression, are presented. Dimuons from Υ and J/ψ resonances, as hard jets and photons, can be observed with enough statistics, efficiency and purity in heavy ion collisions.

На будущем большом адронном коллайдере предполагается проведение экспериментов на встречных пучках адронов с энергией 14 ТэВ и ядер с энергией 5,5–7 ТэВ/нуклон. Высокая светимость и(или) большая множественность событий приведут к необходимости работать в условиях сильной загрузки трекерной системы и калориметра. Необходима разработка методов поиска струй, которые могут работать как в протон-протонных событиях, так и в столкновениях тяжелых ионов, устойчивы по отношению к загрузке и корректируют нелинейность отклика калориметра. В данном обзоре приведены методы выделения струй с использованием комбинации трекерной и калориметрической системы, а также метод вычитания наложенных событий в калориметре. Также рассмотрен ряд измерений, связанных с изучением подавления выхода жестких струй и кваркониев, которые предполагается провести на установке CMS в ядро-ядерных взаимодействиях.

INTRODUCTION

In the Large Hadronic Collider (LHC) the energy available in the collisions between the constituents of the protons (the quarks and gluons) is about 10 times that of LEP and the Fermilab Tevatron. In addition, a wide programme on the study of colliding nuclei with the energy 20 times more than that achieved at RHIC is also supposed. The energy range gives for CMS experiment (one of the four experiments foreseen) the possibility of studying events with high multiplicity

[*]E-mail: Olga.Kodolova@cern.ch

both in pp beams ($\sqrt{S} \sim 14$ TeV) and in colliding nuclei ($E \sim 5.5$ TeV/nucleon) [1]. The tremendous problem comes from the occupancy of detectors especially for heavy ion collisions such as from the data flow which reaches the petabytes per year even after all trigger selections. Thus tracking, calorimetry, data taking and analyzing are the challenge for the present state of the science and technology.

1. CMS DETECTOR

CMS detector will have large acceptance for muons [2] which covers almost five units in pseudorapidity from –2.4 to 2.4. A large magnetic field (4 T) allows one to put calorimeters at a distance of about 1.3 m from the beam pipe. The hadron and electromagnetic calorimeters are located inside a coil and cover (including Very Forward Calorimeter) from –5 to 5 pseudorapidity units. Almost 80% of transverse energy will be gathered in this range [3, 4]. Calorimeter design also allows one to look for the hard jet production and the hard photon measurements in a wide pseudorapidity region. In addition, CMS detector will have precise silicon tracker which gives momentum resolution better than 0.4% for low p_t tracks (p_t less than a few tens of GeV) [5]. The momentuim resolution degrades to 1% for charged particles with momentum greater than 100 GeV.

1.1. Calorimeter Segmentation. In the barrel and the most of the endcap part of HCAL, the size of the tower is $\Delta\eta = 0.0870$ by $\Delta\phi = 2\pi/72 \approx 0.0873$. At high η in the HCAL endcap ($\eta > 1.74$), the towers become larger in η and a double size in ϕ. The granularity of crystals in the ECAL barrel is $\Delta\eta \times \Delta\phi = 0.0175 \times 0.0175$ which corresponds to a crystal front face $\simeq 20 \times 20$ mm. In the ECAL endcap ($1.48 < |\eta| < 3.0$) the η, ϕ granularity increases progressively to a maximum value of $\Delta\eta \times \Delta\phi = 0.05 \times 0.05$, while the crystal size remains the same. There is no longitudinal segmentation in the ECAL and the barrel part of the HCAL. The HCAL endcap has 2 or 3 segments in depth.

CMS calorimeter responses are simulated using detailed calorimeter description in GEANT3 [6]. For the reconstruction of the energy deposition in the hadron calorimeter a calibration constants [7] obtained for the hadron shower model GHEISHA (in GEANT3) have been used. They have been determined with $E_t = 50$ GeV pions at $0.05 < \eta < 0.3$ for the barrel and at $1.8 < \eta < 2.2$ for the endcap part of the calorimeters. The GEANT cuts were 1 MeV for electrons and photons and 10 MeV for hadrons.

1.2. Tracker Detectors. Starting from the beam axis, the tracker is composed of two different types of detectors: the pixel layers and the silicon strip counters. The pixel detector consists of three barrel layers located at 4, 7, 11 cm from the beam axis with granularity 150×150 μm and two forward layers with the granularity 150×300 μm located at a distance of 34 and 43 cm in Z from the centre of detector.

Silicon strip detectors are divided on inner and outer ones and fill tracker area from 20 to 110 cm (10 layers) in transverse direction and up to 260 cm (12 layers) in longitudinal direction. The strip length for silicon strip counters varies up to 21 cm for outermost layers and the pitch varies from 61 to 205 μm depending on radii.

2. CMS OBSERVABLE

The various physics signatures of the processes that CMS is going to observe in pp collisions require that CMS be able to reconstruct and measure final states involving the following:

- charged leptons: electrons, muons, taus;
- jets coming from high-momentum quarks and gluons;
- jets from b quarks;
- missing transverse energy carried off by weakly interacting neutral particles such as neutrino;
- the electroweak gauge bosons; photons, Z, W bosons (in both their dijets and lepton + missing ET modes).

Concerning the heavy ion physics programme on LHC, the primary goal is to study the plasma of quarks and gluons (QGP). The critical temperature for deconfinement $T_c \sim 170{-}260$ MeV depending on the scenario is expected to be reached with heavy ion beams ($E \sim 5.5$ TeV/nucleon) [8]. One of the strongest signatures proposed for QGP evidence is the heavy quark vector mesons suppression [9]. At the same time, the detection of the $Z \to \mu^+\mu^-$ will provide a good reference to estimate the suppression as long as the point-like Z boson is supposed to remain unchanged even at the very high energy densities expected [10]. The other hard probe of QGP is the jet production, as the energy loss of the gluon(quark) in traversing dense matter leads to a quenching, i.e., a suppression of high E_t jets. The dijet quenching, azimuthal anisotropy and enhancement of the monojet/dijet ratio [11, 12] as well as the study of jets in $Z+$jet [10] and $\gamma+$jet [13] channels are possible probes we intend to investigate.

Although CMS detector was designed for the pp interactions but some of its features give good possibility of searching for the hard probes of deconfinement described above.

3. JET MEASUREMENTS IN pp INTERACTIONS

The resolution and linearity with which we will be able to recover energy is a key of importance as it is connected with separation of signal events and background ones and so improving signal/background ratios. One has to mention

that as background we consider both physical background from the channels with the same signature in detector as signal one and fake jets due to pile-up events or high event multiplicity.

Thus reconstruction of jets is performed in at least two steps. The first step is to find jet in calorimeter by means of one of the available procedures. For pp collisions we mainly use iterative cone algorithm [14], and for heavy ion interactions the modified window or cone jet finder [15, 16] was designed (the detailed description of the modified window jet finder see in chapter 5). As soon as jet is found we need to take into account the effects that affect the jet energy and resolution described below.

3.1. Factor's Influence on Jet Reconstruction. Let us consider factors that influence the reconstructed jet energy. These factors can be clearly divided into two groups. The first one is connected with physics of such object as jet:

- fragmentation model of jet;
- initial and final state radiation;
- underlying event-particles coming from other interacting partons;
- in the case of pile-up particles coming from additional minimum bias events.

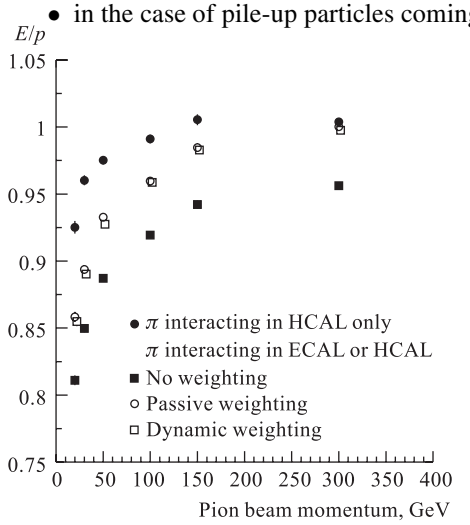

Fig. 1. Linearity of HCAL and ECAL+HCAL response from the test beam data [17]

The other factors connected with detector performance can be considered as:

- electronic noise which should be subtracted somehow from the calorimeter response;
- magnetic field which deflects low energy charge particles out of the jet reconstruction cone;
- different response of neutral and charged particles; as we do not know for each concrete jet ratio between charged and neutral components;
- losses due to out-of-cone showering;
- dead materials and cracks;
- longitudinal leakage for high energy jets.

One should stress that CMS calorimeter consists of two different compartments which have different response for neutral and charged particles. Nonlinearity of HCAL detector achieves 15% as it was learnt during test beam measurements. Ratio energy of beam to the reconstructed energy is presented in Fig. 1, assuming that for e this ratio is equal to one in all dynamical range [17].

The correction for the effects of the first group should be left for the concrete process investigation. As for the detector effect, it could be considered more or less independent of physics process, and common correction coefficients can be provided.

3.2. Energy Correction Algorithms for Calorimeter Jets. Algorithms for jet energy corrections are divided by means of objects that are used for corrections.

Jet Based. Corrections are implemented by means of additional weights to calorimeter longitudinal compartments:

$$E = a \times (\mathrm{EC} + \mathrm{HC}), \tag{1}$$

$$E = a \times \mathrm{EC} + b \times \mathrm{HC}. \tag{2}$$

These weights (*a, b*) depend on (η, E_t) and are tuned for the objects they are referred to (jets of different origin, Missing E_t, etc.). However, the studies showed that this method in the case of CMS gives an improvement in linearity but the resolution is not changed essentially [18, 19]. One or more coefficients give approximately the same result.

Cluster Based. $E = em + hd$, calibration coefficients are applied separately to electromagnetic and hadronic clusters.

Use of Reconstructed Tracks. The main idea is to replace the energy of the calorimeter cluster produced by the charged track with the momentum of track reconstructed in tracker.

1) Energy of jet gathered inside the jet reconstruction cone does not include the tracks that are swept from the cone due to magnetic field. Momenta of these tracks being reconstructed in the tracker $E_{\text{out-of-cone}}$ can be added to the jet response $R_{\text{in-cone}}$ in the calorimeter (Fig. 2):

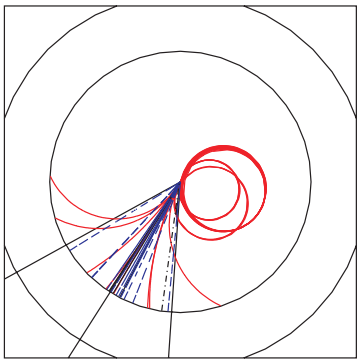

Fig. 2. Jet in CMS calorimeter (transverse plane view)

$$E_{\text{jet}} = R_{\text{in-cone}} + E_{\text{out-of-cone}}.$$

2) For all charged reconstructed tracks one can use measured momenta in the tracker and subtract the expected response of these particles from the jet energy response in the calorimeter. Then the energy of jet is considered as a sum of responses of e/γ and neutral hadrons and momenta of charged hadrons:

$$E_{\text{jet}} = \mathrm{EC}(e/\gamma) + (\mathrm{EC} + \mathrm{HC})(\text{neutral hadrons}) + \text{tracks (charged hadrons)}.$$

3) In the case of a good track-calorimeter cluster matching replace the cluster energy by the track momentum.

The first method «jet based» is very useful on the level 1 trigger where there is no possibility of performing reconstruction in tracker. However, already on the high level trigger we can suppose that regional finder of tracks can be available. The full scale usage of the tracker information for energy corrections can be performed for the off-line jets. A considerable improvement of the calorimeter jet energy resolution with the usage of the reconstructed tracks (energy flow algorithm) has been already demonstrated in a number of HEP experiments at LEP [20], Tevatron [21], DESY [22], Tesla [23]. At present the usage of tracker information is intensively developed for CMS jet calorimetry [24] and is found to be perspective.

3.3. Jet Energy Corrections Using Tracker. Using tracker with CMS calorimeter we can perform different kinds of corrections mentioned above using them both independently and in different combinations. The reconstructed charged tracks that are swept away from the jet cone because of magnetic field can be always added to the jet energy gathered in calorimeters. Part of charged tracks gives separated clusters (energy flow objects) in calorimeter. Thus, if its position coincides with predicted impact on the ECAL surface of the charged particle and the energy of this cluster does not deviate more than two sigmas from the energy of charged track, we can replace the cluster energy in jet response by the track momentum. This method gives an advantage in the case of low multiplicity and tiny granularity of calorimeter. But in the jet cone the particles come close to each other and their showers in calorimeter are overlapped. In this case we can estimate the expected response of the charged particle in the calorimeter and subtract this value from the jet response. The last procedure can work even in the case of highly occupied calorimeter or in calorimeter with rough granularity. In present paper the description of these three procedures is presented and finally the example of their combined usage is shown.

3.3.1. Energy Flow Objects. An algorithmic part of how to build the clusters with the CMS calorimeter and tracker was proposed originally in [25]. The first performance studies of the energy flow method made in [25] looks very promising. The method in [25] is presented with dijet mass reconstruction for $Z' \to jj$ events.

Calorimeter Clusters. The transverse size of the clusters produced by the charged pions has been analyzed from the test beam data [17] with a set-up close to that proposed for CMS. It was found that the most of the energy of pions interacting in the ECAL is contained in 3×3 array of crystals and 3×3 array of HCAL towers behind ECAL. Transverse shape in 3×3 array of crystals (for example weighted transverse radius) does not allow an effective discrimination between pions and electrons. Information in HCAL behind ECAL cluster is then proposed to be used for electron(photon)/pion discrimination when energy flow objects are build.

The clustering begins in the electromagnetic calorimetry, ECAL, as it has the finest granularity. It started from the largest E_t crystal and stopped as soon as there are no neighboring crystals with transverse energy above 0.2 GeV. All crystals that participate in a cluster are removed from the further clustering.

The information on depth is used to sort the ECAL clusters into two categories. Energy in the hadronic calorimeter compartment (HCAL) behind the ECAL seed is added in a 3×3 HCAL tower array if the found HCAL transverse energy is greater than 30% of the ECAL cluster energy. This value is picked using test beam data [17] for pions interacting in the ECAL compartment. If there is no HCAL deposit, then the cluster is considered to be a neutral particle (photon or electron). If there is a match, the cluster is considered to be a charged or neutral hadron which interacted in the ECAL compartment.

When the ECAL energy is exhausted, the remaining HCAL energy is ordered in E_t. The seed in HCAL (HCAL tower) has adjacent 3×3 HCAL towers clustered similarly to the ECAL clustering. The process is terminated when the seed tower E_t falls below 0.2 GeV.

The result of this clustering is a cluster energy, E_t weighted centroid in (η, ϕ), and a particle flag. The flag is 0 if the ECAL cluster has no associated HCAL energy. It is 1 if there is associated HCAL energy of at least 30% of the ECAL energy. Finally, the flag is 2 if there is only HCAL energy without sufficient associated ECAL energy. The last category is assumed to be a charged or neutral hadron interacted only in the HCAL.

Cluster-Track Matching. Only tracks with $|\eta| < 2.4$ and transverse momentum p_t, greater than 1 GeV, are considered. These cuts approximate the angular coverage of the CMS tracker and the lowest transverse momentum not curled up by the magnetic field (loopers). The «looper» transverse momentum to strike ECAL is 0.78 GeV. Deviations of the swum tracks from the calorimeter clusters are calculated taking the cluster error to be 0.087 (HCAL tower size) for both ϕ and η. Matching in energy assumes a dominant calorimeter error with a 100% stochastic term and a 5% constant term [17]. Tracks that are within the calorimeter resolution (tower size) in η and ϕ at the HCAL radius are first merged and their momenta added when considering a match to a calorimeter tower. This procedure allows for matches in the dense core of jets where charged tracks overlap within a calorimeter tower.

A match between the calorimeter cluster and the tracks is defined to exist if $|\Delta\eta|$ is less than the one HCAL tower size, if $|\Delta\phi|$ is less than the two HCAL tower sizes, and if the difference between track momentum and calorimeter cluster energy is between -1 and $+3$ sigma of calorimeter resolution. The offset is due to the observation that the calorimeter energies are systematically lower than the track momenta. In the case of multiple matches, the match with the lowest «chi squared» is taken. If a match exists in all three kinematics variables, the calorimeter cluster is replaced by the matching track. A new flag is defined to

be $= 3$ if this replacement is made. Tracks which would never reach the barrel, «loopers», are added back into the «energy flow» list and a flag $= 4$ is set.

The end result is an energy flow list consisting of unmatched calorimeter clusters (flag $= 0$, 1, or 2), matched (merged) tracks (flag $= 3$), and tracks which would not reach barrel calorimeter (flag $= 4$).

The data set to test the energy flow method is 120 GeV Z' bosons decaying into light quarks with initial state and final state radiation turned on. Events are fully simulated and digitized in detail with CMS simulation and reconstruction packages for luminosity $L = 2 \cdot 10^{33}\ \mathrm{cm}^{-2} \cdot \mathrm{s}^{-1}$. The tracks used in this study are not actual CMS tracks but the PYTHIA generated charged particles. Given that the tracking momentum resolution is much better than the calorimeter energy resolution, this approximation should not alter qualitative conclusions which are made. These tracks are swum in a uniform axial magnetic field to a radius corresponding to the front face of the ECAL. The event-by-event z position of the vertex is used in the swim.

The data used for dijet mass reconstruction is either calorimeter clusters or a hybrid energy flow set consisting of unmatched clusters plus matched tracks and unobserved track loopers. The largest cluster serves as a seed for the first jet. The next highest E_t cluster at a distance $> 2R$ from the first seed is defined to be the seed for the second jet. The vector sum of all the fragments defines the momentum of the jet. The clusters are assumed to be massless. The dijet mass is calculated for the two largest transverse momentum clusters. The calculation is done both for pure calorimeter clusters and for the energy flow list consisting of unmatched clusters, matched tracks, and barrel loopers. Cone size $R = 0.9$ is taken for the jet energy reconstruction.

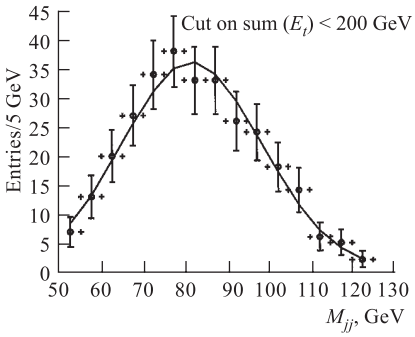

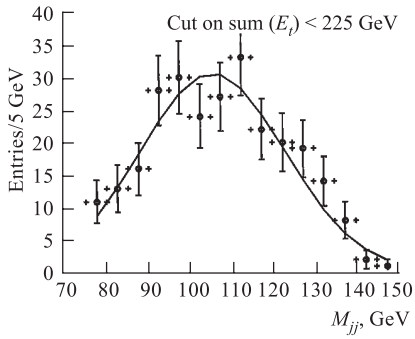

Fig. 3. Dijet mass for $Z' \to jj$ events ($M_{Z'} = 120$ GeV) reconstructed with calorimeter clusters

Fig. 4. Dijet mass for $Z' \to jj$ events ($M_{Z'} = 120$ GeV) reconstructed with the energy flow objects: unmatched clusters, matched tracks and unobserved track loopers

The distribution in dijet mass computed using only calorimeter cluster is shown in Fig. 3. The distribution calculated using all the available information from calorimetry and tracking is shown in Fig. 4.

Gaussian fits are made to the histogrammed data. The mean and sigma for the reconstruction with the calorimeter clusters only are $\langle M_{jj} \rangle = 81.7 \pm 1.1$ GeV and $\sigma_{M_{jj}} = 17.1 \pm 1.0$ GeV. For the reconstructing with energy flow objects the values are $\langle M_{jj} \rangle = 105.5 \pm 1.4$ GeV and $\sigma_{M_{jj}} = 17.8 \pm 1.1$ GeV. We can conclude that mass resolution is improved from 21.0 to 16.9% with the usage of the energy flow objects.

The method may be also very useful to improve missing transverse energy resolution. It requires reconstruction of all the tracks in the event.

3.3.2. Adding of Out-of-Cone Tracks to Jet. This method was described in [24] for the first time. A relatively soft p_t tracks can be swept away from the jet reconstruction cone by 4 T magnetic field. For example track with $p_t = 1.6$ GeV (produced in the pp interaction point) is deflected by the magnetic field on $\Delta\phi = 0.5$ radian from the original direction when it reaches the calorimeter surface. Tracks with $p_t \leqslant 0.8$ GeV don't reach barrel calorimeter at all. In this section we describe a first step towards full usage of tracks in the jet energy measurement: adding energy of the out-of-cone tracks measured with the tracker to the energy of the jet measured with the calorimeter. We define out-of-cone track as a track satisfying the following criteria:

$$\Delta R_v < R_{\rm rec}, \quad \Delta R_c > R_{\rm rec},$$

where $R_{\rm rec}$ is a cone size used for the jet finding with the calorimeter; ΔR_v is a distance in η, ϕ space between calorimeter jet axis and track direction in the production vertex; ΔR_c is a distance between jet axis and an expected impact point of the track on the calorimeter surface.

Effect of adding of the out-of-cone tracks on the jet energy resolution has been studied using QCD 2-jet events generated with PYTHIA 6.152 [26].

The algorithm presented below uses tracks reconstructed by pixel detectors. The pixel lines from the signal vertex only are considered as seeds for the global track finder. Pixel line is defined as a track reconstructed with the pixel detector only. Algorithm of the pixel line reconstruction and vertex finding with the pixel lines is described in [27]. For the track reconstruction we use Combinatorial Track Finder with default settings [28]. Signal vertex (SV) is defined as a vertex with maximal $\Sigma|p_t^i|$ of the pixel lines attached to the vertex.

The present algorithm steps to add out-of-cone tracks are the following:

- reconstruct all pixel lines and vertices from the pixel lines;
- use pixel lines from the SV and within the cone $R_{\rm rec}$ (cone size for the calorimeter jet finder) around the calorimeter jet direction as seeds for the Combinatorial Track Finder;

- find impact points of the reconstructed tracks on the surface of the calorimeter (ECAL);
- add to the calorimeter jet energy the scalar sum of p (momentum) of the tracks with impact points outside the jet reconstruction cone and recalculate η, ϕ of the jet taking into account added tracks.

Figure 5 shows transverse jet energy resolution as a function of E_t of the Monte Carlo jet with $|\eta_{\rm jet}| < 0.5$ for three cases: calorimeter jet energy resolution; with adding of the Monte Carlo out-of-cone tracks of any p_t; with adding of the reconstructed out-of-cone tracks.

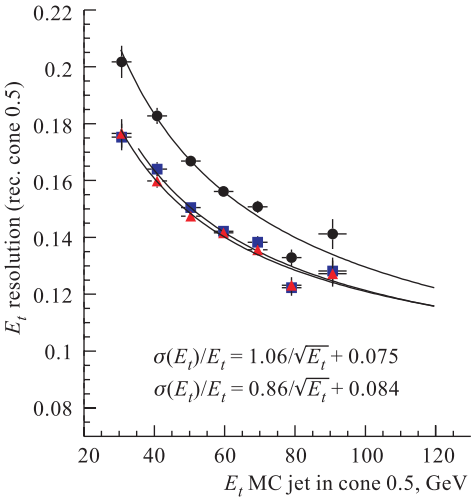

Fig. 5. Jet energy resolution with calorimeter only — circles, after adding of out-of-cone Monte Carlo charged tracks — triangles, after adding of out-of-cone reconstructed tracks — squares. Jets are considered with $|\eta| < 0.5$

One can see that adding of the out-of-cone tracks improves jet E_t resolution by about $10{-}15\%$ and the improvement is more visible for the soft jets of $E_t \sim 30{-}40$ GeV. The improvement is almost the same when the Monte Carlo or reconstructed tracks are being added. It means first, that the usage of the very soft tracks of $p_t < 0.9$ GeV does not improve further jet E_t resolution and second, that the track finding inefficiency is low enough in order not to degrade the performance of this algorithm. Figures 6 and 7 show the jet E_t resolution for the jets in pseudorapidity regions $1.0 < |\eta_{\rm jet}| < 1.5$ and $1.5 < |\eta_{\rm jet}| < 2.2$. One can see that the improvement of the resolution is more visible in the barrel part of the calorimetry $|\eta_{\rm jet}| < 1.5$ which can be explained by the fact that the bigger fraction of the jet energy escapes reconstruction cone in the barrel than in the endcap due to 4 T field. Formulas shown in Figs. 5, 6, and 7 are parameterization of the jet E_t resolution for the calorimeter jets and the jets with the usage of the out-of-cone reconstructed tracks.

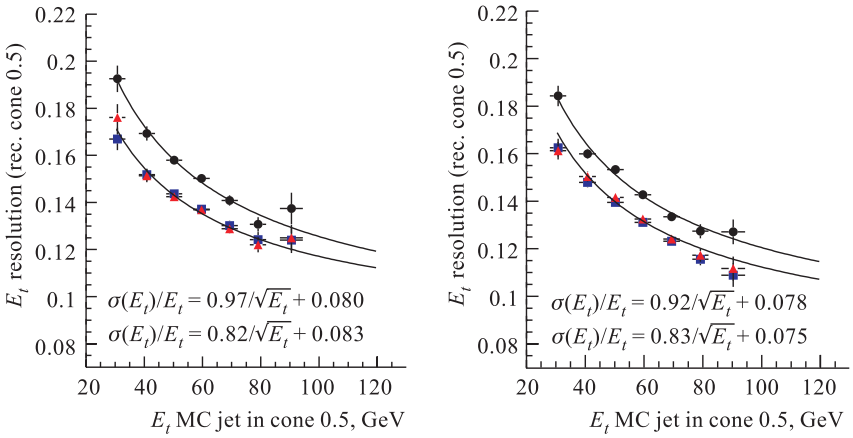

Fig. 6. The same as in Fig. 5 for jets with $1.0 < |\eta| < 1.5$

Fig. 7. The same as in Fig. 5 for jets with $1.5 < |\eta| < 2.2$

3.4. Response Subtraction Algorithm. This method was described in [24] for the first time.

3.4.1. Simulated Data. Samples of QCD dijet events in different intervals of p_t are simulated with PYTHIA 6.152. Jets are found firstly on the generation level (stable particles, including muons and neutrinos) with a simple cone algorithm PYCELL [26] and cone size 0.5. Further these jets will be referred to as Monte Carlo jets (MC jets). Then only one MC jet is taken and the particles which belong to this jet passed through detector simulation; other particles in QCD event are ignored. The detailed calorimeter hit digitization is done for no pile-up scenario.

Calorimeter level jets are reconstructed with the cone 0.5 (as MC jets) using the default calorimeter calibration on the single pion as described above. The comparison of the reconstructed jet is performed for the MC jet. So we pay main attention to the detector effects excluding in some sense effects of initial and final state radiations as well as underlying and pile-up events.

3.4.2. Calculation of Expected Response. The main problem we are faced is how precise we can calculate the expected response. Two different methods have been tried and the both are based on the measurements made with single or isolated particles.

e/π Technique. One can calculate expected response from e/π ratio of the charged hadrons measured for different energy with a set of isolated particles [25]. It can be done during the data taking. We also have to evaluate the ratio of energy that particle leaves in ECAL and HCAL. The response in ECAL is different if

Table 1. **Expected response for charged particles**

	Particle interacts in ECAL	Particle does not interact in ECAL
R_{ECAL}	$E_t \cdot 0.4/(e\pi)_{\mathrm{ECAL}}$	E_{MIP}
R_{HCAL}	$E_t \cdot 0.6/(e\pi)_{\mathrm{HCAL}}$	$(E_t - E_{\mathrm{MIP}})/(e/\pi)_{\mathrm{HCAL}}$

particle interacts in ECAL or not. We separate interacted and noninteracted particles with the energy deposited in 3×3 crystals. If $E_{3\times3} < 0.5$ GeV, we consider particle as noninteracted. The expressions for expected response for charged particles are shown in Table 1. For each charged particle the e/π ratio in ECAL and HCAL is calculated with expressions [25]:

$$(e/\pi)_{\mathrm{ECAL}} = (e/h)_{\mathrm{ECAL}}/(1 + ((e/h)_{\mathrm{ECAL}} - 1) \times F0_{\mathrm{ECAL}}), \tag{3}$$

$$(e/\pi)_{\mathrm{HCAL}} = (e/h)_{\mathrm{HCAL}}/(1 + ((e/h)_{\mathrm{HCAL}} - 1) \times F0_{\mathrm{HCAL}}), \tag{4}$$

where $(e/h)_{\mathrm{ECAL}} = 1.6$, $(e/h)_{\mathrm{ECAL}} = 1.39$ are obtained by fitting test beam data of 300 GeV pion beam [25]. $F0_{\mathrm{ECAL}}$, $F0_{\mathrm{HCAL}}$ are electromagnetic fraction of hadronic shower and can be evaluated with logarithmic dependence: $F0_{\mathrm{ECAL/HCAL}} = 0.11 \ln(E_{\mathrm{ECAL/HCAL}})$ [25]. We took ratio $E_{\mathrm{ECAL}}/E_{\mathrm{HCAL}} = 0.4/0.6$ obtained from the analysis of the test beam data for 300 GeV pion beam [29]. Although the value of the ratio $E_{\mathrm{ECAL}}/E_{\mathrm{HCAL}}$ depends on the energy of particle, we use the constant value in our calculations for the moment.

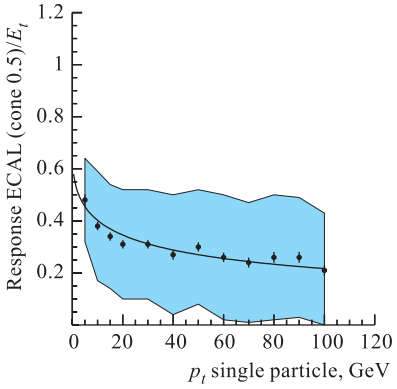

Fig. 8. Mean response in ECAL for isolated charged particles interacted in ECAL in dependence on particle energy. Shadow area corresponds to one dispersion

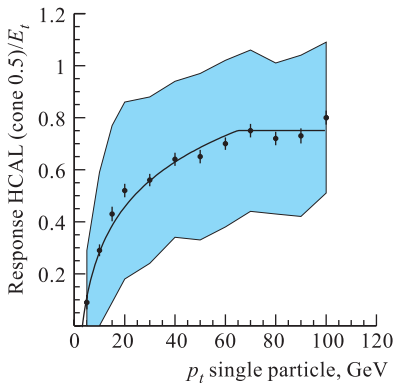

Fig. 9. Mean response in HCAL for isolated charged particles interacted in ECAL in dependence on the particle energy

Library of Responses. Mean responses in ECAL and HCAL corresponded to the interacted in ECAL, and not interacted in ECAL particles are measured with a set of isolated particles of different energies. Initial energy of particle is taken from track reconstruction [28]. Dependence of mean responses in ECAL and HCAL of isolated particles interacted in ECAL is shown in Figs. 8, 9 for isolated particles interacted in ECAL and in Fig. 10 for particles noninteracted in ECAL.

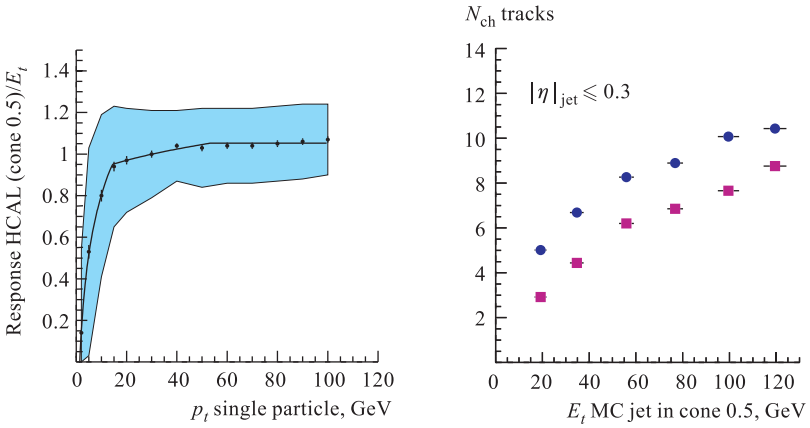

Fig. 10. Mean response in HCAL for isolated charged particles noninteracted in ECAL in dependence on particle energy

Fig. 11. The mean number of generated (•) and reconstructed (■) tracks in jet depending on jet energy

3.4.3. Jet Energy Correction with Response Subtraction. On the first step we find jet in the calorimeter with iterative cone algorithm and determine the position of primary vertex with pixel detectors. For simplification we generate all jets in the point (0, 0, 0). Further we reconstruct tracks in the cone 0.5 at the level of vertex around jet axis. Figure 11 shows the dependence of the reconstructed and generated tracks in a jet at the jet energy. For the 20 GeV jets we loose 50% of charged tracks; and for 100 GeV jets, around 10%.

Nevertheless, the linearity of jet response is improved so as the jet energy resolution (Figs. 12, 13). For 20 GeV jets the resolution is 33% when only calorimeter information is used and 23% when charged tracks found in tracker are added. For 100 GeV jets the resolution diminishes from 12 to 10.6%. The best result is achieved with library of responses. However, one can see from Figs. 8–10 that the distribution of response in calorimeter is rather wide. Now we take the most probable values of the distribution. The more exact shape of the response dependence on the particle energy can be found by means of fitting the known mass like Z or W in their two-jets decay mode or $\gamma/Z+$jet sample.

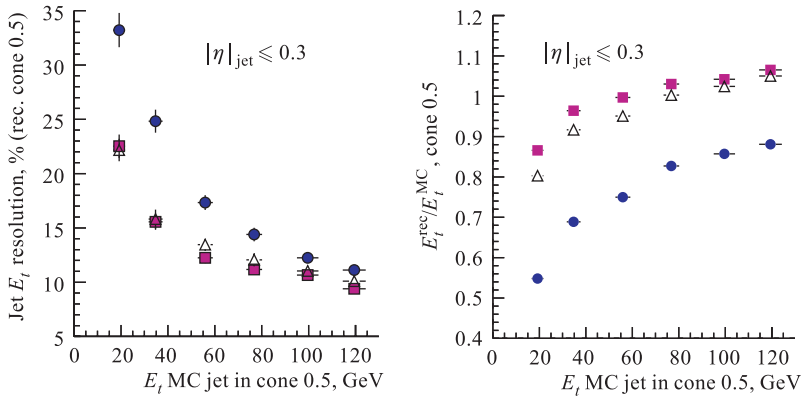

Fig. 12. Dependence of jet energy resolution on MC jet energy: only calorimeter responses (●), subtraction procedure of expected responses using e/π technique and out of cone tracks (△), subtraction procedure of expected responses using library of responses and out of cone tracks (■)

Fig. 13. Dependence of reconstructed jet energy on MC jet energy. The points are the same as in Fig. 12

3.4.4. Combined Response Subtraction and Cluster Matching Algorithm. As is written above cluster matching algorithm and response subtraction can be used in the combination. To suppress the effect of the tracker inefficiency we do not run reconstruction of the tracks but use the information from the generator level supposing the 100% efficiency of tracker:

Jet is found in calorimeter (R_{jet}) and on generation level in cone 0.5 (MC jet).

All charged tracks in cone 0.5 follow until they hit calorimeter surface.

Matrix of 3×3 crystals and 3×3 towers is built around the entry point of charged track.

Sum of energy from 3×3 crystals and 3×3 towers is checked if it coincides with momentum of charged track found in tracker within the following window:

$$-\sigma < (E_t - E_{\text{cal}}) < 2\sigma, \tag{5}$$

where

$$\sigma/E = 100\%\sqrt{(E)} + 5\%. \tag{6}$$

If the energy coincides, then track is called matched and one extracts energy of matrix from the R_{jet} and add the energy of track from tracker instead. The procedure begins from the track with the highest energy.

If the track is not matched (condition for matching is not satisfied), then we calculate the expected response of this track in calorimeter and subtract it from the $R_{\rm jet}$ adding the energy of charged track instead.

For low energy jets, tracks from jets have large distance in between because of the magnetic field. So less amount of cluster overlaps occur and thus more clusters can be considered as matched then for jets with higher energy.

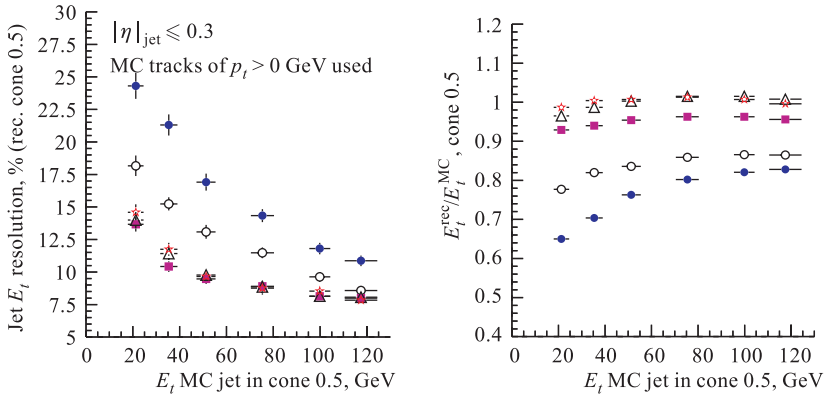

Fig. 14. Dependence of jet energy resolution on MC jet energy: only calorimeter responses (●), out-of-cone tracks are added to calorimeter response (○), subtraction procedure of expected responses using e/π technique and out-of-cone tracks (△), subtraction procedure of expected responses using library of responses and out-of-cone tracks (■), matched tracks and library of responses and out-of-cone tracks (★)

Fig. 15. Dependence of reconstructed jet energy on MC jet energy. The points are the same as in Fig. 14

Finally, out-of-cone tracks are also added to the energy of jet. Dependence of jet energy resolution and jet energy linearity on the MC jet energy is presented in Figs. 14, 15 for four different cases. The first one corresponds to the case when expected response subtraction procedure is used and expected response is evaluated with e/π technique. In the second case, expected response is calculated with the library of responses and in the third case, full correction with track matching, library of responses is performed. Out-of-cone tracks are added for all three cases. Open circles correspond to the case when only out-of-cone tracks are added to calorimeter energy. Including only out-of-cone tracks gives already an essential part of the possible improvement. Different corrections with exchanging charged to the energy response of tracker give the same improvement for resolution, but the best linearity can be achieved with track-cluster matching, library of responses, and out-of-cone tracks. However, the library of responses used here overestimated the response of the particles.

4. JET MEASUREMENTS IN HEAVY ION COLLISIONS

The following signals of jet quenching due to medium induced energy loss are identified as being observable with CMS detector:

• the suppression of high-p_t jet pair in comparison with what is expected from an independent nucleon–nucleon interaction model; it includes modification of impact parameter dependence [30] and azimuthal anisotropy of jet flow in noncentral collisions [31];

• the p_t balance between jet and tagging particle ($Z+$jet [13] or $\gamma+$jet [10]);

• the suppression of high-p_t particle (leading) inside jet;

• the modification of dimuon spectra of semileptonic decays of B and D mesons.

One has to note that jet is found in a fixed cone. The collisional energy loss leads to direct pushing particles out of cone. The radiative loss is the cause of softening of particle spectrum. As a result, more particles are swept out of cone due to magnetic field, and underestimating energy in CMS calorimeter for the low p_t particles leads also to response diminishing.

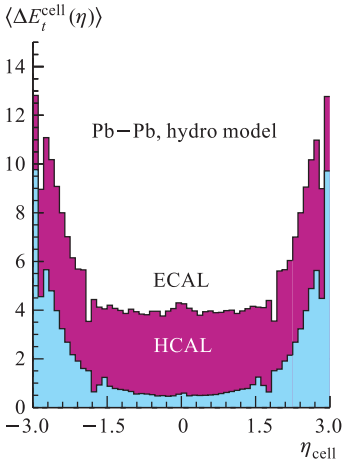

Fig. 16. Dependence of energy deposition in ECAL and HCAL on η for 8000 charged particles per rapidity unit

4.1. Jet Reconstruction in Heavy Ions. Various predictions give the large theoretical uncertainty for the charged particle multiplicity in heavy ion collisions. For Pb–Pb central event, for example, one can expect from 3000 to 8000 of charged particles per rapidity unit in maximum. In this condition the CMS calorimeter is completely occupied. The dependence of the mean energy on η for the 8000 charged particles per rapidity unit is shown in Fig. 16. The distribution is not uniform. The energy deposited in the forward region is much higher than in the central part. Thus if we take iterative cone algorithm without any modification [32], we will find a lot of jets in the forward region which will be completely false. The modified window algorithm was designed specially for the condition of the large energy deposition in calorimeter [15, 16].

• Average transverse energy $\langle E(\eta) \rangle$ and dispersion $D(\eta)$ are calculated for all calorimeter cells as function of η;

• Sliding window consisting of the integer number of cells corresponding to radius R (this is the parameter of algorithm) is constructed;

• The energy of window is calculated as a sum of E_t of all cells contributed to this window minus background energy which is calculated:

$$E_t^{\text{wind}} = \sum_{Nc} E_t^{\text{cell}} - [\langle E_t^{\text{cell}}(\eta)\rangle + D_t^{\text{cell}}(\eta)]; \tag{7}$$

• The nonoverlapping windows with $E_t^{\text{win}} > E_t^{\text{cut}}$ are considered as jet candidate;

• The cell with maximal energy in the window is considered as centre of jet independently where it is located inside window. All cells in a cone with radius R_{cone}, which can differ from the size of window, are considered as cells of jet;

• Average transverse energy $\langle E(\eta)\rangle$ and dispersion $D(\eta)$ are recalculated with cells outside of jets;

• Jet energy is recalculated using new values $\langle E(\eta)\rangle$, $D(\eta)$.

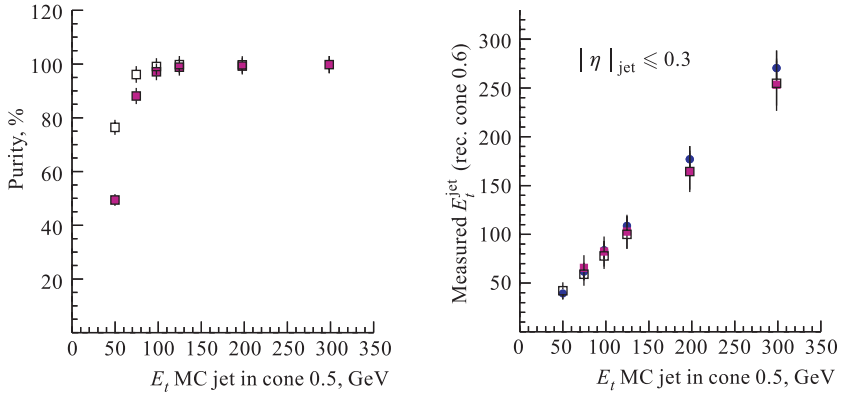

Fig. 17. The efficiency of reconstruction of the true jet vs generated transverse jet energy for different charged particles multiplicities of background event: $(dN_{\text{ch}})/dy = 3000$ (□); $(dN_{\text{ch}})/dy = 8000$ (■)

Fig. 18. The ratio of reconstruction of transverse jet energy to generated transverse jet energy vs generated transverse jet energy: without background (•); $(dN_{\text{ch}})/dy = 3000$ (□); $(dN_{\text{ch}})/dy = 8000$ (■)

The performance of algorithm is checked with central Pb–Pb events generated using simple hydrodynamical model [33]. The mean number of charged particles corresponds to 3000 and 8000 of charged particles per unit of rapidity. The purity of the reconstructed jet sample is presented in Fig. 17. The ratio of the reconstructed jet transverse energy to generated $E_t^{\text{rec}}/E_t^{\text{gen}}$ on the generated transverse energy does not depend on charged particle multiplicity in event (Fig. 18). We observe the degradation of the space resolution (Figs. 19, 20). However, the

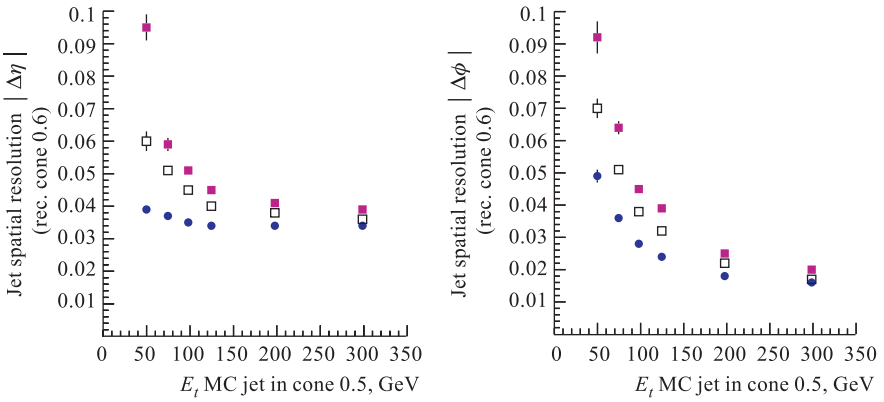

Fig. 19. The η resolution vs generated transverse jet energy. The points are the same as in Fig. 18

Fig. 20. The ϕ resolution vs generated transverse jet energy. The points are the same as in Fig. 18

space resolution is still better than the size of the calorimeter tower. The energy resolution is degraded up to 1.3 times on increasing multiplicity of event to 8000 charged particles per rapidity unit [16].

The fact that mean energy (obtained with the algorithm) does not depend on multiplicity is very important if one intends to normalize spectra (based on jets) to the *pp* case or lower multiplicities (i.e., the other species, centrality and so on). In such a case there is no necessity to include the additional «pile-up» correction factor. The degradation of the jet energy resolution has to be taken into account on comparison spectra obtained with different multiplicity conditions.

4.2. Jet Quenching Observation with $\gamma +$ Jet Channel. The p_t balance between jet and tagging particle γ or Z gives the possibility to estimate energy loss of hard parton. However, both these channels provide some methodical problems. $Z +$ jet channel is good for observation from the background point of view but the rate of $Z +$ jet events is very low. We can have a large rate of $\gamma +$ jet events but background from jet–jet events with a leading π^0 has to be reduced. Figure 21 shows the difference between E_t^{jet} and E_t^{γ} obtained using detailed γ trigger and jet energy resolution found with detailed simulations [16]. The distribution is asymmetric and one has to follow the position of maximum to evaluate parton energy loss. There is still background from π^0 after all calorimeter isolation criteria. We suppose to include tracker information for further background suppression.

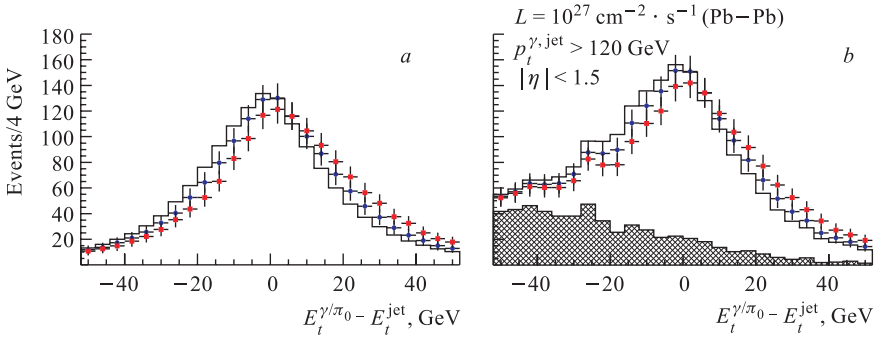

Fig. 21. Difference between E_t of photon and E_t of jet without background (*a*) and with background (*b*). Solid line — $\langle \Delta E \rangle = 0$ GeV; • — $\langle \Delta E \rangle = 4$ GeV; ■ — $\langle \Delta E \rangle = 8$ GeV

4.3. Jet Quenching Observation with Azimuthal Asymmetry. The azimuthal anisotropy of jet and high-p_t particle production in semicentral heavy ion collisions is predicted as effective signal of partonic energy loss in azimuthal nonsymmetric volume of quark-gluon plasma [11, 31, 34]. The methodical advantage of azimuthal jet observable is that one needs to reconstruct only azimuthal position of jet but not the total energy. The summarized in paper [35] present methods for determination of the reaction plane angle are applicable for studying anisotropic flow of soft and semihard particles in current heavy ion experiments at SPS [36], RHIC [37] and might be useful at LHC [31]. If the azimuthal distribution of particles is described well by the elliptic form:

$$\frac{dN}{d\phi} = \frac{N_0}{2\pi}[1 + 2v_2 \cos 2(\phi - \phi_{\mathrm{reac}})], \qquad (8)$$

where N_0 is the number of particles and the coefficient v_2 is an average over particle cosine of 2ϕ, the nuclear reaction plane can be determined as

$$\tan(2\phi_{\mathrm{reac}}) = \frac{\sum_i w_i \sin 2\phi_i}{\sum_i w_i \cos 2\phi_i}. \qquad (9)$$

The weights w_i are selected to optimize the resolution. The weights can be introduced as energy deposition in calorime-

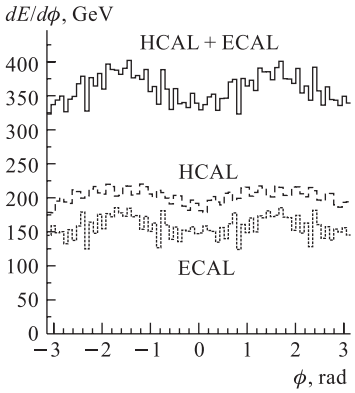

Fig. 22. Dependence of energy in tower on ϕ of tower

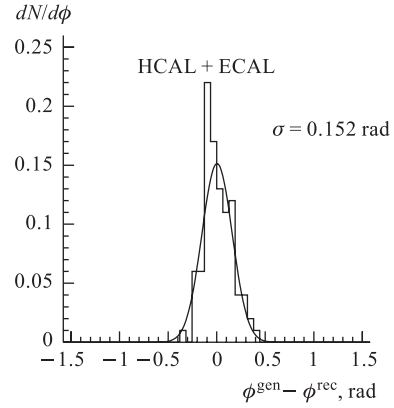

Fig. 23. Dependence between generated and reconstructed azimuthal angles of reaction plane

ter towers. Figure 22 illustrates the energy deposition in calorimeter towers in barrel and endcap regions for Pb–Pb collisions at impact parameter 6 fm generated by the hydrodynamical model. The detector responses are obtained with detailed detector simulation. The estimated resolution of event plane determination 0.15 rad (Fig. 23) allows one to measure the coefficient of azimuthal anisotropy $\cos(2\phi_{\rm jet})$. Recently the method for measurement of jet anisotropy without the event-by-event reconstruction of the reaction plane has been suggested [38]. The detailed investigations of possibility of observing azimuthal anisotropy with CMS detector is presented in [39].

5. IMPACT PARAMETER MEASUREMENT IN HEAVY ION COLLISIONS

It is extremely important to perform different event measurements in dependence on the event centrality. Under the CMS conditions one of the most appropriate way for impact parameter determination is to calculate the transverse energy deposition $E_t^{\rm tot}$ in calorimeters. The strong decrease of the energy deposition from central to peripheral collisions in very forward calorimeter is shown in Fig. 24 for different nuclei (Ca, Nb, Pb) [40]. The simulation of nuclei event

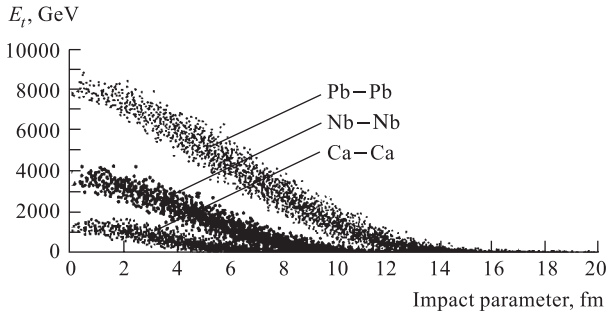

Fig. 24. Dependence of the transverse energy in HF on the impact parameter for different nuclei

is performed with HIJING [41]. The Gaussian width of the impact parameter distribution at fixed energy deposition so as the relative error depending on the value of impact parameter is presented in Fig. 25. The dispersion increases by a factor of two for very peripheral ($b > 13$ fm) events due to diminution of the energy produced in the explored pseudorapidity region.

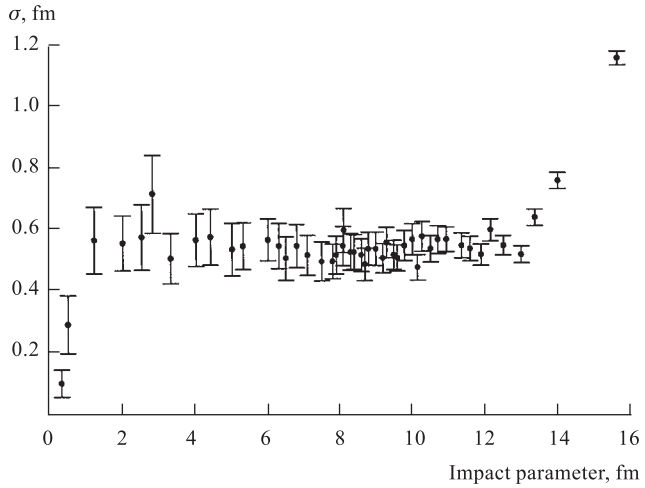

Fig. 25. Resolution on the impact parameter of event

6. VECTOR MESON PRODUCTION IN HEAVY ION COLLISIONS

One of the important signatures of the quark-gluon plasma is the suppression of heavy quark–antiquark resonances [42]. As CMS detector is situated well for the muon identification and measurement, we intend to investigate the production of Υ and J/ψ families through their decay into muons. One of the important tasks is to recognize real Υ in the condition of highly occupied tracker due to very high multiplicity of event. Uncorrelated decays from soft pions and kaons are the main cause of mismatching muons and so the source of the false reconstructed pairs.

6.1. General Conditions for Background and Signal Simulation. Hard processes (heavy resonances) are superimposed on the «thermal» background events. Resonance suppression in the dense matter is not included. Cross sections for the hard events are rescaled from the pp ones:

$$\sigma_{AA} = A^{2\alpha}\sigma_{pp} \tag{10}$$

with $\alpha = 0.9$ for (J/ψ), $\alpha = 0.95$ for (Υ). The cross sections in pp collisions are evaluated using PYTHIA event generator and extrapolation from CDF data [43].

Soft particles (mainly pions and kaons) generated in the heavy ion collisions are one of the important sources of background [44], dominating at the Pb–Pb central events, in the dimuon mass spectrum. The most crucial parameters are multiplicity and transverse momentum distribution of particles.

The most pessimistic cases are considered. Up to 5000 charged particles per unit of rapidity in the central Pb–Pb collision with pseudorapidity shape distribution according to HIJING are taken; and for transverse momentum spectrum the SHAKER [45] parametrization is used. The next source of background for the dimuon spectrum are pairs from the bb and cc decays and also mixed cases when one muon is from the one source and the other from another source; bb and cc decay events are generated with PYTHIA 5.7.

Both «thermal» and hard events are passed through full geant simulation of the CMS detector including all material interactions with low thresholds.

6.2. Dimuon Production. Reconstruction algorithm [46] based on the $\delta\phi, p_t$ roads has been developed for central rapidity region ($|y| < 1.2$). This procedure allows one to find heavy resonances with efficiency from 90 to 75% depending on the event multiplicity (up to 8000 charged particles per rapidity unit, i.e., 60000 particles in CMS acceptance) and suppress at the same time uncorrelated pairs from pions and kaons in 6 times for $|\eta| < 0.8$ and in 2 times for $0.8 < |\eta| < 1.2$. Other background sources mentioned above are also suppressed in comparison with the hard events. Dimuon mass spectrum in the Υ mass range (Fig. 26) is built using all combinations of the track pairs from those achieved in the muon stations and with applying the reconstruction efficiency depending on the track pair origin. The contribution from the different background sources is shown on the same plot. The largest contribution comes from uncorrelated pion and kaon decay into muon.

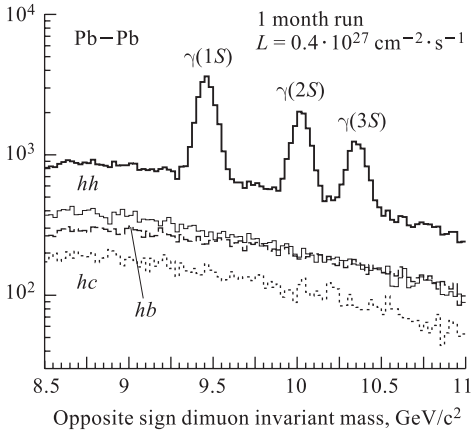

Fig. 26. Dimuon mass spectrum. Minimum bias Pb–Pb events were used in condition of high multiplicity assumption ($dN_{\rm ch}/dy = 5000$ in mid-rapidity region)

Signal/background ratio and number of events are given for one month running time with luminocity 4×10^{26} cm$^{-2} \cdot$ s^{-1} in Tables 2, 3 for Υ for barrel part only and for full acceptance of the detector and for J/ψ (Table 4) for barrel part of detector supposing high (up to 5000 charged particles in rapidity unit) multiplicity case.

Table 2. **Signal/background ratio and event rate of the Υ for the barrel part of detector (high multiplicity assumption)**

	Pb	Sn	Kr	Ar
S/B	3.7	7.8	16.7	100
N_{event}	10000	65000	140000	600000

Table 3. **Signal/background ratio and event rate of the Υ for the barrel and endcap parts of detector (high multiplicity assumption)**

	Pb	Sn	Kr	Ar
S/B	0.4	0.9	1.9	7.3
N_{event}	22000	150000	320000	1400000

Table 4. **Signal/background ratio and event rate of the J/ψ for the barrel part of detector (high multiplicity assumption)**

	Pb	Sn	Kr	Ar
S/B	1.3	3.4	7.9	35
N_{event}	5800	40000	100000	400000

Large statistics will give the possibility of investigating the dependence on the impact parameter of the event and transverse momentum of the resonances.

Uncorrelated background can be extracted using like-sign dimuon spectrum:

$$S = OS - 2\sqrt{N^{++}N^{--}} \tag{11}$$

where subtraction is made in each bin of the dimuon opposite-sign spectrum (Fig. 27).

In the high invariant mass region $M(\mu^+\mu^-) > 20$ GeV Drell–Yan, Z boson and semileptonic decays of the open flavors (cc, bb) are the main sources of the dimuons. Using cut for the p_t of muon more than 5 GeV/c makes contribution of the uncorrelated decays from the soft particles negligible. A clear signal of Z into $\mu\mu$ decays is seen [10]. The expected number of the Z decays is 11000 and the expected number of $Z+$jet events is 900 for the one month Pb–Pb run assuming 50% of accelarator efficiency, i.e., $1.3 \cdot 10^6$ s and luminocity 10^{27} cm$^{-2} \cdot$ s^{-1}.

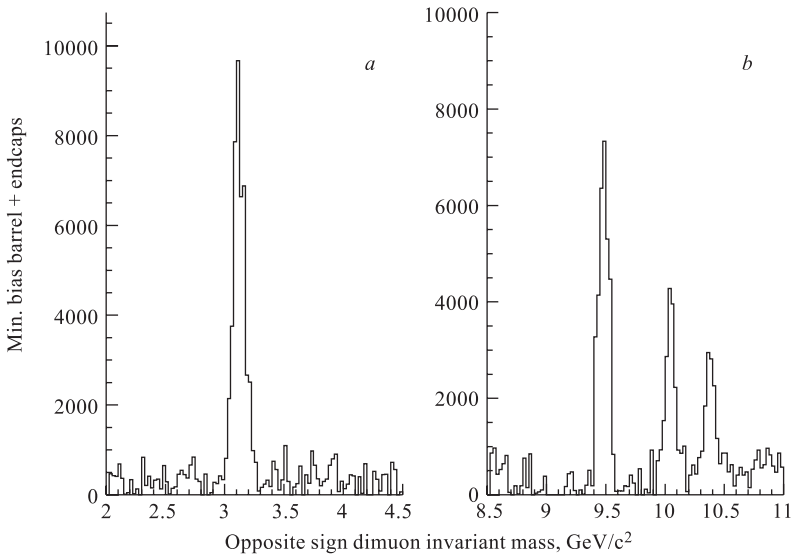

Fig. 27. Dimuon mass spectrum after background subtraction

CONCLUSIONS

Various physics channels that are going to be observed require the possibility of identifying and measuring muons, electrons, gamma, jets both in pp and in heavy-ion collisions. At present different algorithms are developed for jet and muon measurements.

For pp physics it is extremely important to have a good jet energy resolution and linearity of jet reconstruction. The new perspective method to correct jet energy combining the information from calorimeters and tracker detectors using response subtraction algorithm was supposed to be used in CMS. The algorithm is useful for calorimeters with rough granularity and high occupancy of calorimeter cells. It gives improvement of jet resolution 1.5 times for 20 GeV jets and 15% for 100 GeV jets and at the same time significantly improves linearity of jet energy collection.

In heavy ion collisions calorimeters are completely occupied and it is impossible to use the same iterative cone algorithm for jets reconstruction as for pp events. A new pile-up subtraction algorithm was developed in CMS. Jets are observable with good efficiency and purity above 75 GeV threshold. It appears that this algorithm is also very important for high luminosity ($L = 10^{34}\ \mathrm{cm}^{-2} \cdot \mathrm{s}^{-1}$) pp collisions for rejecting fake low E_t jets. $\gamma +$ jet and $Z +$ jet events give the possibility of estimating medium induced parton energy loss. However, the problem of background and statistics still remains.

The new perspective way to study jet quenching is to take advantage of good jet spatial resolution and calculate the azimuthal anisotropy which can be done both with detector plane determination and without.

Due to high multiplicity of the event and occupied tracker, the reconstruction of heavy quark–antiquark resonances through their decay into muons becomes a complicated task. A special dimuon reconstruction algorithm was developed for heavy-ion collisions. With this algorithm Υ can be observed with signal background ratio from 3.7 (Pb–Pb) to 100 (Ar–Ar) in barrel part of CMS detector. The number of events is 7900 and 450000 correspondingly. If we add endcap region, the number of events becomes 18000 and 1020000 and signal/background ratio is 0.4 and 7.3 for the same nuclei. In spite of the low acceptance of detector for J/ψ we can get enough amount of J/ψ to perform correlations study.

Acknowledgments. The author is thankful to I. Vardanyan, A. Nikitenko, D. Green, I. Lokhtin, A. Snigirev, S. Petrushanko, P. Zarubin, R. Kvatadze, M. Bedjidian who provided the material for the paper.

REFERENCES

1. *The LHC Study group*. CERN/AC95-05-LHC.
2. CMS MUON Design Report. CERN/LHCC 97-32. 1997.
3. CMS ECAL Design Report. CERN/LHCC 97-33. 1997.
4. CMS HCAL Design Report. CERN/LHCC 97-31. 1997.
5. CMS Tracker Design Report. CERN/LHCC 98-6. 1998.
6. CMSIM User's Guide at www.http://cmsdoc.cern.ch/swsi.html
7. *Kunori S.* http://home.fnal.gov/∼kunori/cms_sw/colo_sw/hcal_hits_digi.html
8. *Laermann E.* // Nucl. Phys. A. 1996. V. 610. P. 1;
   Boyd G. et al. // Nucl. Phys. B. 1996. V. 469. P. 419.
9. *Matsui T., Satz H.* // Phys. Lett. B. 1986. V. 178. P. 416.
10. *Kartarilishvili V., Kvatadze R., Shanidze R.* // Phys. Lett. B. 1995. V. 356. P. 589.
11. *Wang X.-N.* // Phys. Rev. C. 2001. V. 63. 054902.
12. *Lokhtin I. P. et al.* CMS NOTE-1998/025. 1998.
13. *Wang X.-N., Huang Z., Sarcevic I.* // Phys. Rev. Lett. 1996. V. 231. P. 77.
14. *Breitweg J. et al. (ZEUS Collab.)* // Eur. Phys. J. C. 1998. V. 2. P. 61.
15. *Accardi A. et al.* Hard Probes in Heavy Ion Collisions at the LHC: Jet Physics. hep-ph/0310274.
16. *Kodolova O. L. et al.* CMS NOTE-1998/063. 1998.
17. *Abramov V. et al.* // Nucl. Instr. Meth. A. 2001. V. 457. P. 75–100.
18. *Kodolova O. et al.* CMS NOTE-2002/023. 2002.
19. *Abdullin S. et al.* CMS IN-2001/001. 2001.
20. See for example *Buskulic D. et al. (ALEPH)* // Nucl. Instr. Meth. A. 1995. V. 360. P. 481–506.

21. *Lami S. et al.* FERMILAB-Conf-00/342-E CDF. 2001.

22. *Wing M.* Precise Measurement of the Jet Energies with the ZEUS Detector // Proc. of the IX Intern. Conf. on Calorimetry in Part. Phys., Annecy, Oct. 9–14, 2000.

23. *Gay P.* Energy Flow // Proc. of the Linear Collider Workshop 2000, Fermilab, Batavia, IL, USA, 2000; http://www-lc.fnal.gov/lcws2000

24. *Green D. et al.* CMS NOTE-2002/036. 2002.

25. *Green D.* Energy Flow in CMS Calorimetry. Fermilab-FN-0709.

26. *Sjostrand T.* // Comp. Phys. Commun. 1994. V. 82. P. 74.

27. *Cucciarelli C. et al.* CMS NOTE 2003/026. 2003.

28. The Trigger and Data Acquisition Project. Technical Design Report. CMS TDR 6.2. 2002. V. 2.

29. *Freeman J.* Private communication.

30. *Lokhtin I. P., Snigirev A. M.* // Eur. Phys. J. C. 2000. V. 16. P. 527.

31. *Lokhtin I. P., Petrouchanko S. V., Sarycheva L. I.* // Proc. of the Intern. Conf. on Physics and Astrophysics of Quark-Gluon Plasma, Jaipur, India, Nov. 26–30, 2001; Phys. At. Nucl. 2002. V. 65. P. 943.

32. *Abe F. et al. (CDF Collab.)* // Phys. Rev. D. 1992. V. 45. P. 1448.

33. *Kruglov N. A. et al.* // Z. Phys. C. 1997. V. 76. P. 99.

34. *Gyulassy M., Levai P., Vitev I.* // Nucl. Phys. B. 2000. V. 197. P. 571; Phys. Rev. Lett. 2000. V. 85. P. 5535; Nucl. Phys. B. 2001. V. 594. P. 371.

35. *Voloshin S. A., Zhang Y.* // Z. Phys. C. 1996. V. 70. P. 665;
Pokanzer A. M., Voloshin S. A. // Phys. Rev. C. 1998. V. 58. P. 1671.

36. *Appelshauser H. et al. (NA49 Collab.)* // Phys. Rev. Lett. 1998. V. 80. P. 4136.

37. *Ackermann K. H. et al. (STAR Collab.)* // Phys. Rev. Lett. 2001. V. 86. P. 402;
Snellings R. J. et al. (STAR Collab.) // Nucl. Phys. A. 2002. V. 698. P. 193;
Racey R. A. et al. (PHENIX Collab.) // Ibid. P. 559.

38. *Lokhtin I. P., Sarycheva L. I., Snigirev A. M.* // Phys. Lett. B. 2002. V. 537. P. 261.

39. *Lokhtin I. P. et al.* CMS NOTE-2003/019.

40. *Damgov I. et al.* // Part. Nucl. Lett. 2001. V. 107. P. 93; CMS NOTE 2001/055.

41. *Gyulassy M., Wang X.-N.* // Phys. Rev. D. 1991. V. 44. P. 3501; Comp. Phys. Commun. 1994. V. 83. P. 307.

42. *Bedjidian M. et al.* Hard Probes in Heavy Ion Collisions at the LHC: Heavy Flavour Physics. hep-ph/0311048.

43. *Abe F. et al. (CDF Collab.).* Fermilab-Pub-95/271-E.

44. *Bedjidian M., Drapier O.* CMS NOTE-99/052. 1999.

45. *Antinori F.* Internal note. ALICE/MC. 93-09. 1993.

46. *Kodolova O., Bedjidian M.* CMS NOTE-99/004. 1999.